

# Kinematics and Dynamics of a Continuum Motion-Correction Mechanism for Frameless and Maskless Cancer Radiation Therapy

Olalekan Ogunmolu<sup>†</sup>, Erik Pearson<sup>\*</sup>, Xinmin Liu<sup>\*</sup>, and Rodney Wiersma<sup>\*</sup>

**Abstract**—**TO-DO: Under development**

## I. INTRODUCTION

This paper is a continuation of the constitutive model of a single soft robot, called IABs that we modeled and verified in [1] for use in real-time motion compensation/correction in radiation therapy. Here, we present the systematic analysis of the parallel continuum robots which are manipulators of head and neck (H&N) region of a patient in framless and maskless (F&M) cranial radiosurgery or radiation therapy. Having a real-time closed-loop robotic system that can automatically correct motion deviation, particularly during beam-on time during RT treatment is an RT technological need that has the potential benefits of hastening the current treatment time in clinics, minimizing patient discomfort post-treatment (as opposed to rigid frames and masks used in frame and mask-based RT), and drastically improving dose efficacy so that the patient's treatment can be effectively fractionated. For details on the radiation oncological treatment procedure, we refer readers to [2] and [3].

In this work, we derive the kinematics of a wearable soft continuum mechanism as described in [1] (reproduced in Figure 1) necessary for motion-compensation, as well as planning and control of a patients' H&N motion on a treatment machine. We call the individual soft robots inflatable air bladders (IABs) owing to their hollow internal chamber that admits or ejects air based on an applied pressurization. We make the fundamental assumption that the IAB's deformation follows the isochoric deformation principle, with reasonable local volume preservation during deformation constraints baked into the physical IAB material properties, and we follow the model that we earlier derived in [1] in determining the manipulator map, kinematics, Jacobian and end-effector characteristics. Soft parallel robots are notoriously difficult to control, given their continuum-based mechanical properties, the inter-dependency of the parameters that characterize their deformation, and the individual robot link constraints. It is not

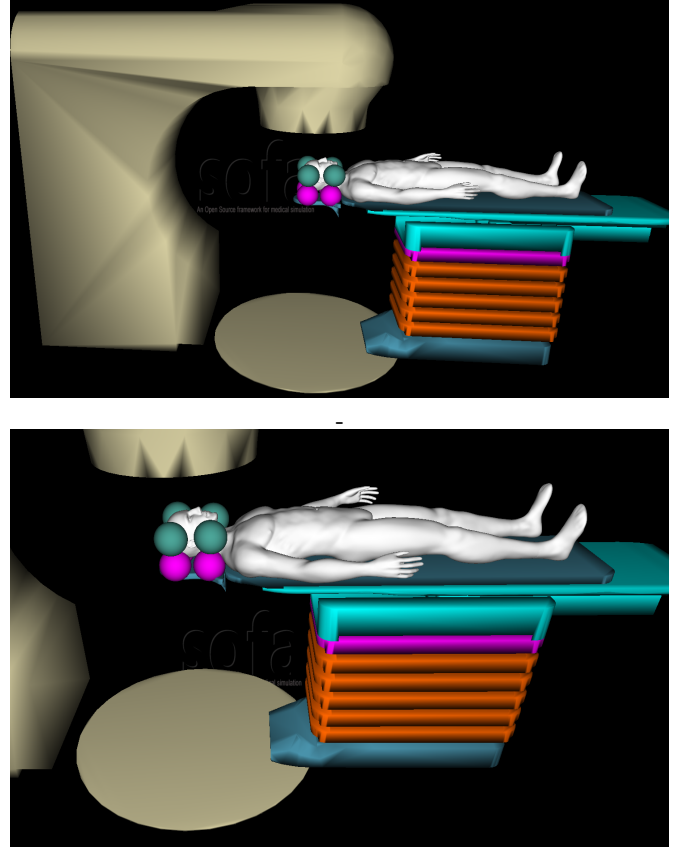


Fig. 1: System setup in the SOFA Framework Architecture. **Top:** Gantry, Turntable, Patient and IAB Chains around the patient's H&N Region. **Bottom:** Close-up view of compensating IABs around patient's H&N region with the patient lying in a supine position on the treatment couch. [Image best visualized in colored ink].

surprising that different schemes for controlling soft continuum robots have appeared in literature with mixed successes [4]–[9]. For an extensive literature review of the control of continuum soft robots, we refer readers to [10].

The soft robot mechanism presented in this work consists of IABs connected with extensible couplings; these couplings are chosen to exploit the soft structures' design for impedance control of the H&N region of the patient. We analyze the manipulation map, the Jacobian of the IAB chains, as well as the contact equations between the IAB mechanism system and patient. This paper is a sequel to the constitutive model

<sup>†</sup>Perelman School of Medicine, The University of Pennsylvania, Philadelphia, PA 19104, USA. ogunmolo@penmedicine.upenn.edu

<sup>\*</sup>Department of Radiation Oncology, The University of Chicago, Chicago, IL 60637, USA. {xmliu, epearson, rwiersma}@uchicago.edu

Research reported in this publication was supported by National Cancer Institute of the National Institutes of Health under award number R01CA227124. Olalekan Ogunmolu conceived, developed and implemented the ideas reported in this paper. Erik Pearson provided the CAD models for the system setup, while Rodney Wiersma advised the authors.

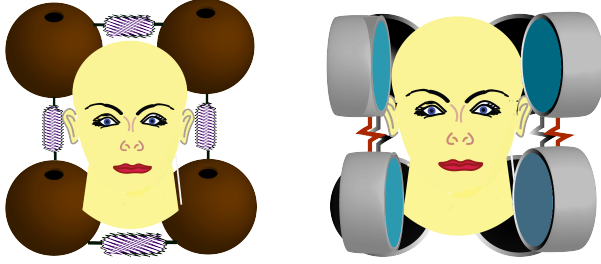


Fig. 2: An abstraction of the patient’s position correction mechanism. In the left image, there are four IABs that constitute the base kinematic chain. They lift the head along the Z-axis as well as provide pitch motion corrections. On the right, the side kinematic chains provide roll and yaw motion corrections. [Image best visualized in colored ink].

presented in in [1]; we expand upon the kinematic configuration of the multi-DOF soft actuation system for H&N motion compensation in RT. Our design goals include a system that (1) provides patient comfort whilst manipulating human body parts necessary for trajectory following during RT, (2) assures dose efficacy while not attenuating the ionizing radiation dose treatment due to undesirable material properties (3) capable of emerging complex morphological computational behavior with deformable soft robots – simplifying complex patient motion planning and control during robotic RT treatment.

**TO-DO:** The rest of this paper is organized as follows: in § II, we briefly review the hardware setup and system configuration, we then analyze the contact kinematics in § III. In § IV, we derive the mechanism’s end-effector velocities and forces, and then derive the Newton-Euler Lagrangian relationship in § V. We present manipulation examples in the SOFA framework in ?? and conclude the paper in § VII. Proofs and derivations are provided in appendices A, B, and C.

## II. SYSTEM DESCRIPTION

Figure 2 illustrates the kinematic arrangement of the soft robots around the head. The geometry of this material has inflatable internal cavities that pressurize under the influence of fluids that flow in or out of the cavities via pneumatic hoses/tubes. The complete setup in a typical radiation oncology treatment room that includes the gantry, couches, turntable, as well as the patient is shown in Figure 1, modeled in the SOFA Framework architecture [11]. The IABs are linked by semi-plastic connectors that allow for passive displacement and orientation to accommodate varying patient head sizes and shapes when one or more of the IABs deform. The system is composed of one closed and two open soft robot kinematic chains.

The range of motions of the kinematic arrangement above give are described in what follows. Take the left symmetry of the robot configuration. This manipulates the cranial region about the  $+x$  axis, while the right kinematic chain manipulates the head about the right-left plane ( $-x$ ). A closed kinematic chain lies underneath the patient’s head, providing actuation about the **TO-DO: anterior-posterior direction: they compensate**

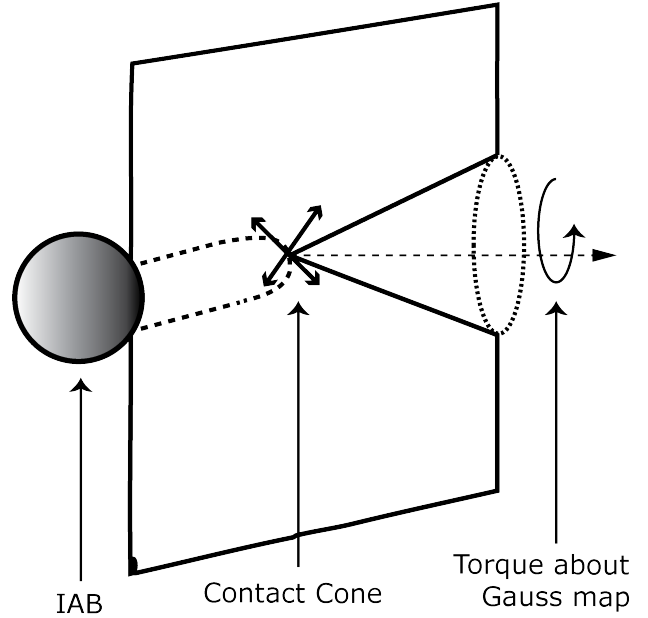


Fig. 3: Illustration of the IAB Soft Contact Type

the head along the z-axis or in a pitch orientation direction. When only two along the sides are actuated, it results in a yaw/y-axis motion of the head. We utilize the four pairs to realize precise translational and rotatory head motions about the z-axis. The connectors between the IABs in each chain are passive, adjustable to accommodate a patient’s head size. **draw axes of translation/rotation here.**

## III. ANALYSIS OF CONTACT KINEMATICS

We describe the contact between an IAB and the head through a mapping between the force exerted by the IAB at the contact point and the resultant forces at the center of mass of the head. We model the contact type between the head and an IAB similar to the soft finger contact primitive of [12]. Here, our soft contact is the convex sum of *point contacts* with friction over the small area of contact. IAB forces and torques are modeled within a “cone of forces” about the direction of the surface normal from a patient’s head (see Figure 3). The trajectory of the head under the influence of motion of an IAB is influenced by the position vector  $\mathbf{r}$  described in [1]. When the IAB deforms, body forces over its current configuration and contact (*traction*) forces over its boundary  $\partial\mathcal{B}$  impact motion on the head. Constrained by the frictional coefficient, we define the soft contact force inside the friction cone as

$$\tilde{\mathbf{F}}_{c_i} = \begin{bmatrix} \mathbf{I} & 0 \\ 0 & n_{c_i} \end{bmatrix} \begin{bmatrix} f_{c_i} \\ \tau_{c_i} \end{bmatrix}, \quad (1)$$

where  $f_{c_i} \in \mathbb{R}^3$  denotes the amount of force exerted by the IAB along the direction of contact,  $\tau_{c_i} \in \mathbb{R}$  is the moment of the contact force, and  $n_{c_i}$  is the *normal* or *Gauss map*<sup>1</sup> for a manifold  $S \subset \mathbb{R}^3$  of a head surface. For contact models with friction, we require that all contact forces lie within the friction

<sup>1</sup>A normal map for a manifold  $S$  is a continuous map  $g : S \rightarrow S^2 \subset \mathbb{R}^3$  such that for every  $s \in S$ ,  $g(s)$  is orthogonal to  $S$  at  $s$  [13].

cone, determined by the friction coefficient. The set of forces within or on the boundary of the friction cone is

$$FC = \{f_c \in \mathbb{R}^n : \|f_{c_{ij}}^t\| \leq \mu_{ij} \|f_{c_i}^n\|, \\ i = 1, \dots, k, j = 1, \dots, m_i\} \quad (2)$$

where  $f_{c_{ij}}^t$  is the tangent component of the  $j^{th}$  element of the contact force,  $f_{c_i}^n$  is  $i^{th}$  contact's normal force, and  $\mu_{ij}$  is  $f_{c_{ij}}$ 's coefficient of friction.

#### A. Boundary Value Problem for IAB Deformation

We now solve the boundary-value problem for the IAB deformation when in contact with the head as a follow-up to our analysis in [1]. Again, we assume a spherically-symmetric deformation constraint imposed on the IAB when the head rolls or slips. This may be achieved via an appropriate vulcanization of the IAB rubber material, for example (see [14] or [15]). We leave the physical design to a future implementation. For a semi-rigid IAB material, when the SoRos are in contact with the head, the applied forces on the current configuration of the IAB body  $\mathcal{B}$  are

- the body forces,  $\mathbf{b}$
- the contact forces,  $f_c$ , at the IAB boundary,  $\partial\mathcal{B}$ , and
- the gravitational force of the head mass acting along the direction of contact,  $f_g$ .

We make the explicit assumption that the head maintains contact with the IAB throughout deformation. Suppose that for the  $i^{th}$  IAB in the chain,  $r_{c_i}$  represents the direction vector perpendicular from the point of contact to the center of the head cone of forces, it follows that the three equations that governs the motion of the IAB continuum are given as

$$\dot{\rho} + \rho \operatorname{div} \mathbf{v} = 0 \quad (3a)$$

$$\boldsymbol{\sigma}^T = \boldsymbol{\sigma} \quad (3b)$$

$$\operatorname{div} \boldsymbol{\sigma}^T + \rho \mathbf{b} = \rho \dot{\mathbf{v}}, \quad (3c)$$

being respectively the conservation of mass (3a), the symmetry of the stress tensor (3b), and the balance of linear momentum respectively, (see [16, pp. 150], for the derivation). In general, we expect that the mass of the body will be conserved given the incompressibility assumption of the IAB material, thus guaranteeing that (3a) is fulfilled. We have from (3c) and the symmetric properties of the stress tensor that

$$\frac{1}{r^2} \frac{\partial}{\partial r} (r^2 \sigma_{rr}) + \frac{1}{r \sin \phi} \frac{\partial}{\partial \phi} (\sin \phi \sigma_{r\phi}) + \frac{1}{r \sin \phi} \frac{\partial}{\partial \theta} (\sigma_{r\theta}) \\ - \frac{1}{r} (\sigma_{\theta\theta} + \sigma_{\phi\phi}) = \rho b_r \ddot{\mathbf{r}}_x \quad (4a)$$

$$\frac{1}{r^3} \frac{\partial}{\partial r} (r^3 \sigma_{r\phi}) + \frac{1}{r \sin \phi} \frac{\partial}{\partial \phi} (\sin \phi \sigma_{\phi\phi}) + \frac{1}{r \sin \phi} \frac{\partial}{\partial \theta} (\sigma_{\theta\phi}) \\ - \frac{\cot \phi}{r} (\sigma_{\theta\theta}) + \rho b_\phi = \rho \ddot{\mathbf{r}}_y \quad (4b)$$

$$\frac{1}{r^3} \frac{\partial}{\partial r} (r^3 \sigma_{r\theta}) + \frac{1}{r \sin^2 \phi} \frac{\partial}{\partial \phi} (\sin^2 \phi \sigma_{\theta\phi}) \\ + \frac{1}{r \sin \phi} \frac{\partial}{\partial \theta} (\sigma_{\theta\theta}) + \rho b_\theta = \rho \ddot{\mathbf{r}}_z \quad (4c)$$

where  $\ddot{\mathbf{r}}_x$ ,  $\ddot{\mathbf{r}}_y$ , and  $\ddot{\mathbf{r}}_z$  are components of the position vector  $\ddot{\mathbf{r}}$  as defined in Appendix B of [2] and the body forces  $b_r, b_\phi, b_\theta$  are

components of the gravitational force of the head acting on the IAB body  $\mathcal{B}$ . If the deformation is spherically symmetric, we expect that the shear stress component contributions  $\sigma_{r\phi}, \sigma_{r\theta}, \sigma_{\phi\theta}$  would vanish in (4). It follows that the forces on the head (see derivation in Appendix § A are in part the internal pressurization, and component stresses  $\{P_i, \sigma_{\phi\phi}(\epsilon), \sigma_{\theta\theta}(\zeta)\}$  as given in (5)

$$P = \int_{r_i}^{r_o} \left[ \frac{1}{r} \left( -2p + 2C_1 \frac{r^2}{R^2} - 2C_2 \frac{R^8}{r^8} \right) - \rho b_r \right. \\ \left. + \rho \cos \theta \left( 2\dot{r}\dot{\phi} \cos \theta + r \cos \theta \ddot{\phi} - 2r\dot{\theta}\dot{\phi} \sin \theta \right) - \rho \sin \phi \right. \\ \left. \left( \cos \theta (-\ddot{r} + r\dot{\theta}^2 + r\dot{\phi}^2) + \sin \theta (2\dot{r}\dot{\theta} + r\ddot{\theta}) \right) \right] dr \quad (5a)$$

$$\sigma_{\phi\phi}(\epsilon) = - \int_{\epsilon}^{\pi} \left[ r\rho \left[ \cos \phi \left( 2r\dot{\theta}\dot{\phi} \cos \theta + (2\dot{r}\dot{\phi} + r\ddot{\phi}) \sin \theta \right) \right. \right. \\ \left. \left. + \sin \theta \left( 2\dot{r}\dot{\theta} \cos \theta + r\ddot{\theta} \cos \theta + (\ddot{r} - r\dot{\theta}^2 - r\dot{\phi}^2) \right) \sin \phi \right] \right. \\ \left. - \rho r b_\theta \right] d\phi, \quad 0 \leq \epsilon \leq \pi \quad (5b)$$

$$\sigma_{\theta\theta}(\zeta) = - \int_{\zeta}^{2\pi} \left[ -r\rho b_\theta \sin \phi + r\rho \sin \phi \cos \phi \left( \ddot{r} - r\dot{\phi}^2 \right) \right. \\ \left. - r\rho \sin^2 \phi \left( 2\dot{r}\dot{\phi} + r\ddot{\phi} \right) \right] d\theta, \quad 0 \leq \zeta \leq 2\pi, \quad (5c)$$

where  $0 \leq \epsilon \leq \pi$ , and  $0 \leq \zeta \leq 2\pi$ .

#### B. Contact Forces, IAB Stress Components, and Head Gravitational Force

Tell readers you are linking the previous section with the stress mechanics to find end effector velocities. We assume that the stress vector  $\boldsymbol{\sigma}$  at a point on the IAB surface is uniform and continuous throughout the IAB boundary so that it linearly depends on the normal map (this follows from Cauchy's theorem; readers may see the proof in [16, §3.3.1]). Recall that the correspondence between material line elements in the reference and current configuration is

$$\mathbf{dx} = \mathbf{F} \mathbf{dX} \implies \mathbf{F}^{-T} \mathbf{dx} = \mathbf{dX}.$$

Let  $\mathbf{H} = \mathbf{F}^{-T}$  and  $\mathbf{dA}$  represent an infinitesimal vector element on the material surface at a neighborhood of point  $\mathbf{X}$  in  $\mathcal{B}$  such that  $\mathbf{dA} = \mathbf{N} dA$ , where  $\mathbf{N}$  is the unit outward normal to the IAB boundary  $\partial\mathcal{B}_o$  in the reference configuration. What is  $\mathbf{dA}$ . The corresponding deformed surface of the IAB with normal  $\mathbf{n}$  from a surface,  $da$ , of the IAB in the current configuration is  $\mathbf{da} = \mathbf{n} da$ . Using Nanson's formula, we have the following relation between surfaces in the reference and current configuration

$$\mathbf{da} = J \mathbf{H} \mathbf{dA} \implies \mathbf{n} da = J \mathbf{H} \mathbf{N} dA. \quad (6)$$

where  $J = \det \mathbf{F}$ . Multiplying throughout equation (6) by the derived constitutive relation between the stress-strain relationship of [1], the resultant contact force on the boundary  $\partial\mathcal{B}$  in the current configuration may be written as (owing to the volume preservation on the boundary of the IAB material)

$$\int_{\partial\mathcal{B}} \boldsymbol{\sigma} \mathbf{n} da = \int_{\partial\mathcal{B}_o} J \boldsymbol{\sigma} \mathbf{H} \mathbf{N} dA. \quad (7)$$





$C_{p_1}$  and  $C_{p_h}$  such that

$$R \frac{\partial f_1}{\partial \alpha_1} M_1^{-1} R_\psi = \frac{\partial f_h}{\partial \alpha_h} M_h^{-1} \quad (15)$$

where  $M_i$  is a  $2 \times 2$  square root of the Riemannian metric tensor [18] that normalizes the columns of  $\frac{\partial f}{\partial \alpha}$ , i.e.

$$M_i = \begin{bmatrix} \|\frac{\partial f_i}{\partial u_i}\| & 0 \\ 0 & \|\frac{\partial f_h}{\partial v_i}\| \end{bmatrix} \quad (16)$$

and  $R_\psi$  is chosen such that a rotation of  $C_{p_1}$  about its  $z$ -axis through  $-\psi$  radians aligns the  $x$ -axes of the local coordinate system  $\alpha_1$  to that of the head's local coordinate system  $\alpha_h$  i.e.

$$R_\psi = \begin{bmatrix} \cos \psi & -\sin \psi \\ -\sin \psi & -\cos \psi \end{bmatrix}. \quad (17)$$

Notice that  $R_\psi = R_\psi^T = R_\psi^{-1}$ . We define the normalized Gauss frame at a point  $u$  on the surface  $U$  of the orthogonal coordinate system  $(f, U)$  as,

$$[x_u \ y_u \ z_u] = [\frac{\partial f}{\partial u} / \|\frac{\partial f}{\partial u}\| \quad \frac{\partial f}{\partial v} / \|\frac{\partial f}{\partial v}\| \quad n_u(f(u))] \quad (18)$$

where  $x_u, y_u$ , and  $z_u$  are functions mapping  $U \subset \mathbb{R}^2 \rightarrow \mathbb{R}^3$  and  $n_u$  is the continuous Gauss map  $n_u : S \rightarrow S^2 \subset \mathbb{R}^3$ . The motion of the contacts  $\dot{\eta}$  as a function of components of the twist vector  $\dot{\xi} = (v, \omega)^T$  is given in (19) as the respective *first*, *second*, and *third equations of contact*. Our derivation, which closely follows [19]'s multi-fingered kinematics' proof, may be found in Appendix B of [2].

$$\dot{\alpha}_h = M_h^{-1} (\mathcal{K}_h + \tilde{\mathcal{K}}_1)^{-1} (\omega_t - \tilde{\mathcal{K}}_1 v_t) \quad (19a)$$

$$\dot{\alpha}_1 = M_1^{-1} R_\psi (\mathcal{K}_h + \tilde{\mathcal{K}}_1)^{-1} (\omega_t - \mathcal{K}_h v_t) \quad (19b)$$

$$\dot{\psi} = \omega_n + T_h M_h \dot{\alpha}_h + T_1 M_1 \dot{\alpha}_1 \quad (19c)$$

where

$$T_h = y_h^T \frac{\partial x_h}{\partial \alpha_h} M_h^{-1}, \quad T_1 = y_1^T \frac{\partial x_1}{\partial \alpha_1} M_1^{-1},$$

$$\mathcal{K}_h = [x_h^T, y_h^T]^T \frac{\partial n_h^T}{\partial \alpha_h} M_h^{-1}, \quad \omega_n = z_h^T \omega$$

$$\mathcal{K}_1 = R_\psi [x_1^T, y_1^T]^T \frac{\partial n_1^T}{\partial \alpha_1} M_1^{-1} R_\psi,$$

$$\omega_t = [x_h^T, y_h^T]^T [n_h \times \omega]^T,$$

$$v_t = [x_h^T, y_h^T]^T [(-f_h \times \omega + v)]^T. \quad (20)$$

Note that  $\omega_t$  is the rolling velocity of the head projected onto the tangent plane of the contact and  $v_t$  is the sliding velocity;  $\omega_n$  is the relative rotational velocity projected to the contact's surface normal, and  $\tilde{\mathcal{K}}_1 = R_\psi \mathcal{K}_1 R_\psi$  is the curvature of the IAB with respect to the contact frame that coincides with the normalized Gauss frame at  $p_1(t)$ . The matrix  $(\mathcal{K}_h + \tilde{\mathcal{K}}_1)^{-1}$  is the so-called *relative curvature* originally coined by [13].

Simplifying (20), we find that

$$\begin{aligned} x_h &= \frac{\partial f}{\partial u_h} / \|\frac{\partial f}{\partial u_h}\|, & y_h &= \frac{\partial f}{\partial v_h} / \|\frac{\partial f}{\partial v_h}\|, & z_h &= n_u(f(u)) \\ T_h &= y_h \left[ \frac{\partial x_h^T}{\partial u_h} / \|\frac{\partial f}{\partial u_h}\|, \frac{\partial x_h^T}{\partial v_h} / \|\frac{\partial f}{\partial v_h}\| \right], \\ T_1 &= y_1 \left[ \frac{\partial x_1^T}{\partial u_1} / \|\frac{\partial f}{\partial u_1}\|, \frac{\partial x_1^T}{\partial v_1} / \|\frac{\partial f}{\partial v_1}\| \right], \\ \mathcal{K}_h &= [x_h^T, y_h^T]^T \left[ \frac{\partial n_h^T}{\partial u_h} / \|\frac{\partial f}{\partial u_h}\|, \frac{\partial n_h^T}{\partial v_h} / \|\frac{\partial f}{\partial v_h}\| \right], \\ \mathcal{K}_1 &= [x_1^T, y_1^T]^T \left[ \frac{\partial n_1^T}{\partial u_1} / \|\frac{\partial f}{\partial u_1}\|, \frac{\partial n_1^T}{\partial v_1} / \|\frac{\partial f}{\partial v_1}\| \right]. \end{aligned} \quad (21)$$

We see that for the contact interaction between an IAB and the head, for a  $U \subset \mathbb{R}^2$  we must choose an appropriate  $f_i : U_i \rightarrow S_i \subset \mathbb{R}^3$  in order to characterize the setup.

#### IV. MULTI-IAB KINEMATICS

At a material point,  $\mathbf{r}$ , of the IAB surface in the configuration  $\mathcal{B}$ , the 3D position of a point based on the radial distance  $r$  from the origin and the angles  $\phi$  and

$$\mathbf{R} = \begin{bmatrix} R \cos \Theta \sin \Phi \\ R \sin \Theta \sin \Phi \\ R \cos \Phi \end{bmatrix} \quad \text{and} \quad \mathbf{r} = \begin{bmatrix} r \cos \theta \sin \phi \\ r \sin \theta \sin \phi \\ r \cos \phi \end{bmatrix}. \quad (22)$$

$\theta$  is given by (22). The configuration space of the IAB with respect to the spatial frame at a certain time can then be described by  $g_{st}(\mathbf{r}) : \mathbf{r} \rightarrow g_{st}(\mathbf{r}) \in SE(3)$  while the strain state of the IAB is characterized by the strain field

$$\hat{\xi}_i(\mathbf{r}) = g_i^{-1} \frac{\partial g_i}{\partial \mathbf{r}} \in \mathfrak{se}(3) = g_i^{-1} g'_i \quad (23)$$

with the respective  $g'_i$ s being the tangent vector at  $g_i$  such that  $g'_i \in T_{g_i(\mathbf{r})} SE(3)$ . For an incompressible IAB, the strain field becomes

$$\begin{aligned} g_i(\mathbf{r}) = \exp^{\|\mathbf{r}\| \hat{\xi}_i} &= \mathbf{I} + \hat{\xi}_i \|\mathbf{r}\| + \frac{\hat{\omega}}{\|\omega\|^2} (1 - \cos(\|\mathbf{r}\| \|\omega\|)) \hat{\xi}_i^2 \\ &+ \frac{\hat{\omega}^3}{\|\omega\|^3} (\|\mathbf{r}\| \|\omega\| - \sin(\|\mathbf{r}\| \|\omega\|)) \hat{\xi}_i^3. \end{aligned} \quad (24)$$

##### A. End Effector Forces

From the derived relationship between the head contact coordinates and the relative motion  $(v_t, \omega_t)$  of the IAB i.e. equation (19), we can associate a Jacobian that maps IAB velocities to head position and orientation. A basic assumption in our formulation is that the IABs make contact with the head throughout manipulation, and the manipulation is stable and prehensile. A forward kinematic map  $K_{iab_i}(\mathbf{r}_i) : \mathbb{R}^{n_i} \rightarrow SE(3)$  maps from respective IAB positions to head position and orientation. The velocity of the head with respect to a fixed base frame in terms of IAB velocities can be written in terms of the forward kinematics Jacobian:

$$\begin{pmatrix} v_{iab_i} \\ \omega_{iab_i} \end{pmatrix} = \frac{\partial K_{iab_i}}{\partial \mathbf{r}_i} \frac{d\mathbf{r}}{dt} K_{iab_i}^{-1} = \mathbf{J}_i(\mathbf{r}_i) \dot{\mathbf{r}}_i \quad (25)$$

where  $\mathbf{r}_i$  is the spatial position of IAB  $i$ , and  $(v_{iab_i}^T, \omega_{iab_i}^T) \in \mathbb{R}^6$  represents the linear and angular velocity of the  $i^{th}$  IAB about its screw basis. In essence,  $\mathbf{r}_i \in \mathbb{R}^3$  with its rows of mapped to

scalars by an appropriate choice of norm. The contact between the head and the IABs is mapped by the Jacobian

$$\mathbf{J}_{c_i}(\xi_h, \xi_{iab_i}) = \begin{bmatrix} \mathbf{I} & \hat{\mathbf{w}}(r_{c_i}) \\ \mathbf{0} & \mathbf{I} \end{bmatrix} \mathbf{J}_{r_i}, \quad (26)$$

where  $\mathbf{J}_{c_i} : \dot{\xi}_{r_i} \rightarrow [v_{c_i}^T, w_{c_i}^T]^T$ ,  $r_{c_i} \in \mathbb{R}^3$  is a vector between the head reference point (e.g. the center of mass) and the contact with the  $i^{th}$  IAB,  $\xi_h$  is the position and relative orientation of the head,  $\xi_{iab_i}$  is the position and relative orientation of the  $i^{th}$  soft robot in world coordinates,  $\hat{\mathbf{w}}(r_{c_i})$  is an anti-symmetric matrix for the vector  $r_{c_i}$ , and  $\xi_r = (\xi_{r_1}, \xi_{r_2}, \dots, \xi_{r_8})$  are the positions and orientations for each of the 8 IABs. The manipulation map,  $G_i$  is made up of matrices of the form

$$G_i(\xi_h, \xi_r) = \begin{bmatrix} \mathbf{I} & \mathbf{0} \\ \hat{\mathbf{w}}(r_{c_i}) & \mathbf{I} \end{bmatrix} B_i(\xi_h, \xi_r), \quad (27)$$

where  $B_i(\xi_h, \xi_r)$  is the selection map as defined in [20] for the desired manipulation. The net force on the head is a sum of the individual forces arising from each IAB. Owing to the linearity of each individual IAB's contact force, the resultant head force can be stitched together to form  $G$ , *i.e.*

$$\tilde{F}_h = [G_1, \dots, G_8] \begin{pmatrix} \tilde{F}_{c_1} \\ \vdots \\ \tilde{F}_{c_8} \end{pmatrix} = G \tilde{F}_c, \quad (28)$$

where  $F_h \in \mathbb{R}^6$  and  $F_c \in \mathbb{R}^{m_1} \times \mathbb{R}^{m_2} \times \dots \times \mathbb{R}^{m_8}$ . The *internal* or *null forces* is captured by the null space  $\mathcal{N}(G)$  of the manipulation map  $G$ ; these forces correspond to zero net force on the head of the patient. Each  $\tilde{F}_{c_i}$  in (28) is of the form (13).

### B. End-effector Velocities

Following [19], we define the velocity constraint dual of (27) as the constraint between the relative velocity of the head and that of the twist velocities of the contact point

$$\begin{pmatrix} \tilde{v}_{c_i} \\ \tilde{\omega}_{c_i} \end{pmatrix} = \begin{bmatrix} \mathbf{I} & \hat{\mathbf{w}}(r_{c_i}) \\ \mathbf{0} & \mathbf{I} \end{bmatrix} \begin{pmatrix} v_{c_i} \\ \omega_{c_i} \end{pmatrix}. \quad (29)$$

For a conjugate twist vector  $(v_c^T, \omega_c^T)^T$  to the the forces exerted by the IABs,  $f_c$ , we have the following

$$\begin{pmatrix} v_c \\ \omega_c \end{pmatrix} = G^T \begin{pmatrix} v_{c_h} \\ \omega_{c_h} \end{pmatrix}. \quad (30)$$

Given a *selection matrix*  $B_i^T(\xi_h, \xi_{iab_i}) \in \mathbb{R}_i^{m_i}$  for a particular manipulation task, where  $m_i$  is the range of all the forces and moments for the chosen contact primitive (or union of contact primitives), the *manipulation map* for the  $i^{th}$  IAB can be written as,

$$G_i^T(\xi_h, \xi_{iab_i}) \xi_h = B_i^T(\xi_h, \xi_{iab_i}) \mathbf{J}_{c_i}(\xi_h, \mathbf{r}_{r_i}) \dot{\xi}_{iab_i} \quad (31)$$

where  $\mathbf{J}_{c_i}$  is the contact Jacobian for the  $i^{th}$  soft robot, and  $\xi_h$  denotes the velocity of the head. In the arrangement of Figure 2, for the 8 soft robots, the manipulation constraint of

the system can be written as

$$\begin{bmatrix} G_1^T \\ G_2^T \\ \vdots \\ G_8^T \end{bmatrix} \begin{pmatrix} v_h \\ w_h \end{pmatrix} = \mathbf{diag} \begin{pmatrix} B_1^T \mathbf{J}_{c_1} \\ B_2^T \mathbf{J}_{c_2} \\ \vdots \\ B_8^T \mathbf{J}_{c_8} \end{pmatrix} \begin{pmatrix} \dot{\mathbf{r}}_{iab_1} \\ \dot{\mathbf{r}}_{iab_2} \\ \vdots \\ \dot{\mathbf{r}}_{iab_8} \end{pmatrix}. \quad (32)$$

In what follows below, we give examples of the composition of the head manipulation map under different scenarios on a treatment table. These would be helpful when we use (31) to determine the head velocity in world coordinates. In these examples, there is an implicit assumption that the angle of tilt of the head around the axis of normal is measurable by a gyroscope or a vision sensor or other sensors of similar facsimile. We show how to find the manipulation map of the head when the IAB kinematic chain underneath the head are passive, and only the four IABs surrounding the head are actuated (see Figure 2) *i.e.* roll motion of the head. We then present finding the manipulation map of the head when all 8 IABs are simultaneously active *i.e.* the pitch, roll and yaw motion of the head.

### V. HEAD-IAB SYSTEM'S NEWTON-EULER EQUATIONS

From the *determinism principle for stress* [21], the Cauchy stress  $\sigma$  at any point in a material at time  $t$  for any motion up to time  $t$  determines the stress response of the material for any arbitrary motion history up to and including time  $t$ . We will derive the dynamics of the IAB system in the *strain field of the deformation*. The potential and kinetic energy of the system are considered to be derived from the constitutive strain field relations that characterize the deformation. We now use Lagrangian deformation analysis to derive the dynamic equations of the continuum multi-IAB system of Figure 2.

The constitutive law which describes the macroscopic IAB material behavior with respect to a reference frame,  $T$ , at a time,  $t$  can be completely characterized by ten dependent variables viz., three components of the position vector, six component stress tensor variables (the shear and normal stress components), and the density,  $\rho$ , of the material [16, §4.1.1].

#### A. Lagrange's Equations

We are interested in the final position and orientation of the IAB as a whole rather than the system of particles that characterize a deformation at every time  $t$ . For a kinetic energy  $T$  and a potential energy  $V$ , the *Lagrangian*,  $L$ , of the system in generalized coordinates is the difference between the kinetic and potential energy, *i.e.*

$$L(\mathbf{r}, \dot{\mathbf{r}}) = T(\mathbf{r}, \dot{\mathbf{r}}) - V(\mathbf{r}). \quad (33)$$

The equations of motion for the pneumatic system is of the form

$$\frac{d}{dt} \frac{\partial L}{\partial \dot{\mathbf{r}}_i} - \frac{\partial L}{\partial \mathbf{r}_i} = \boldsymbol{\tau}_i, \quad i = 1, \dots, m \quad (34)$$

where  $\boldsymbol{\tau}_i$  is the torque acting on the  $i^{th}$  generalized coordinate. Written in matrix form equation (34) becomes

$$\frac{d}{dt} \frac{\partial L}{\partial \dot{\mathbf{r}}} - \frac{\partial L}{\partial \mathbf{r}} = \boldsymbol{\tau}. \quad (35)$$

It now remains to derive the kinetic and potential energies for the IAB material. Let the velocity of an IAB material particle  $\mathbf{x}$  in the current configuration at time  $t$  be  $\mathbf{v}(\mathbf{r}, t)$ , then the Eulerian velocity gradient tensor can be defined as

$$\mathbf{\Gamma} = \text{grad } \mathbf{v}(\mathbf{r}, t). \quad (36)$$

The first law of Cauchy's law of motion will allow us to derive the balance of mechanical energy of the system. Multiplying equation (??) throughout by  $\mathbf{v}(\mathbf{r}, t)$ , and abusing notation by dropping the arguments of  $\mathbf{v}(\mathbf{r}, t)$ , we find that

$$\begin{aligned} & \text{div}(\boldsymbol{\sigma}^T \cdot \mathbf{v}) + \rho \mathbf{b} \cdot \mathbf{v} = \rho \mathbf{v} \cdot \dot{\mathbf{v}} \\ \Rightarrow & \text{div}(\boldsymbol{\sigma}^T \mathbf{v}) - \text{tr}(\boldsymbol{\sigma} \mathbf{\Gamma}) + \rho \mathbf{b} \cdot \mathbf{v} = \rho \mathbf{v} \cdot \dot{\mathbf{v}}. \end{aligned} \quad (37)$$

Following mass conservation, we integrate over volume  $\mathcal{B}$  and employ the divergence theorem, so that the above relation yields the *balance of mechanical energy*:

$$\int_{\mathcal{B}} \rho \mathbf{b} \cdot \mathbf{v} dv + \int_{\partial \mathcal{B}} f_p \cdot \mathbf{v} da = \frac{d}{dt} \int_{\mathcal{B}} \frac{1}{2} \rho \mathbf{v} \cdot \mathbf{v} dv + \int_{\mathcal{B}} \text{tr}(\boldsymbol{\sigma} \mathbf{\Gamma}) dv \quad (38)$$

where  $f_p$  is the IAB body force density, and the left hand side of the foregoing is the so-called *rate of working of the applied forces*. The symmetry of the stress tensor  $\boldsymbol{\sigma}$  implies that  $\text{tr}(\boldsymbol{\sigma} \mathbf{\Gamma}) = \text{tr}(\boldsymbol{\sigma} \mathbf{\Sigma})$  where  $\mathbf{\Sigma}$  is given in terms of the Eulerian-strain rate tensor,  $\mathbf{\Gamma}$  *i.e.*

$$\mathbf{\Sigma} = \frac{1}{2}(\mathbf{\Gamma} + \mathbf{\Gamma}^T) \quad (39)$$

so that the kinetic energy density and stress power are given by,

$$T(\mathbf{r}, \dot{\mathbf{r}}) = \frac{1}{2} \rho \mathbf{v} \cdot \mathbf{v}, \quad V(\mathbf{r}) = \text{tr}(\boldsymbol{\sigma} \mathbf{\Sigma}). \quad (40)$$

The stress-strain relation for the IAB we have presented are only related through the deformation tensor dependence, implying that the material is Cauchy elastic. For Cauchy elastic materials, the stress power term is not conserved during deformation making integration over the material body  $\mathcal{B}$  physically unrealistic [16]. For such materials, we may set the stored strain energy  $V$  to an arbitrary constant (e.g. an identity or  $V(I) = 0$ ). We can derive the overall torque dynamics of an IAB system as

$$\begin{aligned} \boldsymbol{\tau} = & \underbrace{\begin{bmatrix} \rho & 0 & 0 \\ 0 & \rho r^2 & 0 \\ 0 & 0 & \rho r^2 \sin^2 \phi \end{bmatrix}}_{M_{iab}} \begin{bmatrix} \ddot{r} \\ \ddot{\phi} \\ \ddot{\theta} \end{bmatrix} \\ & + \underbrace{\text{diag} \begin{bmatrix} 2\rho r (\dot{\theta} \sin^2 \phi + \dot{\phi}) \\ \rho r (r\dot{\theta} \sin 2\phi - \dot{\phi}) \\ -\rho r \dot{\theta} \sin \phi (r \cos \phi + \sin \phi) \end{bmatrix}}_{C_{iab}} \begin{bmatrix} \dot{r} \\ \dot{\phi} \\ \dot{\theta} \end{bmatrix} \end{aligned} \quad (41)$$

Rewriting equation (41) in terms of the torque for each soft robot in Figure 2, we have the dynamics for IAB  $j$  as

$$M_{iab_j}(r_j, \phi_j) \ddot{\mathbf{r}}_j + C_{iab_j}(r_j, \phi_j, \dot{\theta}_j, \dot{\phi}_j) \dot{\mathbf{r}}_j = \boldsymbol{\tau}_j \quad (42)$$

where  $M_{iab_j}$  and  $C_{iab_j}$  are the respective inertia and Coriolis forces matrices for the soft robot,  $j$  while  $\boldsymbol{\tau}$  is the actuator torque. Since the material of the IAB is incompressible, the mass density is uniform throughout the body of the material. In general, we write equation (42) as

$$M_{iab}(\tilde{\mathbf{r}}) \ddot{\tilde{\mathbf{r}}} + C_{iab}(\tilde{\mathbf{r}}, \dot{\tilde{\mathbf{r}}}) \dot{\tilde{\mathbf{r}}} = \tilde{\boldsymbol{\tau}} \quad (43)$$

where  $\tilde{\mathbf{r}} \in \mathbb{R}^{n_1} \times \mathbb{R}^{n_2} \times \dots \times \mathbb{R}^{n_s}$  gives the generalized coordinates for all the IABs and  $\tilde{\boldsymbol{\tau}}$  are the vectorized torques of the individual robots.

## VI. SYSTEM NEWTON-EULER EQUATIONS

The dynamics of the head is a form of (43) but without the actuator torques. In local coordinates, it has the form

$$M_h(\zeta) \ddot{\zeta} + C_h(\zeta, \dot{\zeta}) \dot{\zeta} + N_h(\zeta, \dot{\zeta}) = 0 \quad (44)$$

with  $\zeta$  being a local parameterization of the position and orientation of the head,  $x_h \in SE(3)$ , and  $N_h$  being the gravitational and frictional forces. The head and the multi-DOF IAB system are connected via manipulation constraint *i.e.*

$$G^T(\zeta, \mathbf{r}) \dot{\zeta} = \mathbf{J}(\zeta, \mathbf{r}) \dot{\mathbf{r}}. \quad (45)$$

Suppose that the velocity constraint produces a virtual displacement constraint in  $\delta \zeta$  and  $\delta \mathbf{r}$  such that for  $q = (\zeta, \mathbf{r})$ , we have

$$\delta \mathbf{r} = \mathbf{J}^{-1}(q) G^T(q) \delta \zeta$$

the Lagrange equations become

$$\left( \frac{d}{dt} \frac{\partial L}{\partial \dot{q}} - \frac{\partial L}{\partial q} - (\boldsymbol{\tau}, 0) \right) \delta q = 0 \quad (46)$$

$$\left( \frac{d}{dt} \frac{\partial L}{\partial \dot{\mathbf{r}}} - \frac{\partial L}{\partial \mathbf{r}} - \boldsymbol{\tau} \right)^T \begin{pmatrix} \delta \mathbf{r} \\ \delta \zeta \end{pmatrix} = 0 \quad (47)$$

$$\begin{aligned} & \left( \frac{d}{dt} \frac{\partial L}{\partial \dot{\mathbf{r}}} - \frac{\partial L}{\partial \mathbf{r}} - \boldsymbol{\tau} \right) \delta \mathbf{r} + \left( \frac{d}{dt} \frac{\partial L}{\partial \dot{\zeta}} - \frac{\partial L}{\partial \zeta} \right) \delta \zeta = 0 \\ GJ^{-T} \left( \frac{d}{dt} \frac{\partial L}{\partial \dot{\mathbf{r}}} - \frac{\partial L}{\partial \mathbf{r}} - \boldsymbol{\tau} \right) \delta \zeta + \left( \frac{d}{dt} \frac{\partial L}{\partial \dot{\zeta}} - \frac{\partial L}{\partial \zeta} \right) \delta \zeta &= 0 \end{aligned} \quad (48)$$

from where

$$\left( \frac{d}{dt} \frac{\partial L}{\partial \dot{\zeta}} - \frac{\partial L}{\partial \zeta} \right) \delta \zeta + GJ^{-T} \left( \frac{d}{dt} \frac{\partial L}{\partial \dot{\mathbf{r}}} - \frac{\partial L}{\partial \mathbf{r}} \right) = GJ^{-T} \boldsymbol{\tau} \quad (49)$$

given the arbitrariness of  $\delta \zeta$ . Equations (49) alongside (45) completely describe the system.

## VII. CONCLUSION

TO-DO: To be developed.

## APPENDIX A IAB DYNAMICS

We now derive the overall dynamics for the elastic IAB in Eulerian form. Following (22), a point on the surface of the IAB has the following Cartesian description

$$\begin{aligned} \mathbf{r} &= \begin{bmatrix} x \\ y \\ z \end{bmatrix} = \begin{bmatrix} r \cos \theta \sin \phi \\ r \sin \theta \sin \phi \\ r \cos \phi \end{bmatrix} \\ \dot{\mathbf{r}} &= \begin{bmatrix} \dot{x} \\ \dot{y} \\ \dot{z} \end{bmatrix} = \begin{bmatrix} \dot{r} \cos \theta \sin \phi - r \dot{\theta} \sin \theta \sin \phi + r \dot{\phi} \cos \theta \cos \phi \\ \dot{r} \sin \theta \sin \phi + r \dot{\theta} \cos \theta \sin \phi + r \dot{\phi} \sin \theta \cos \phi \\ \dot{r} \cos \phi - r \dot{\phi} \sin \phi \end{bmatrix} \end{aligned} \quad (50)$$

and the components of  $\ddot{\mathbf{r}}$  are

$$\begin{aligned} \ddot{x} &= \cos \theta \left( 2\dot{r}\dot{\phi} \cos \theta + r \cos \theta \ddot{\phi} - 2r\dot{\theta}\dot{\phi} \sin \theta \right) \\ &\quad - \sin \phi \left( \cos \theta \left( -\ddot{r} + r\dot{\theta}^2 + r\dot{\phi}^2 \right) + \sin \theta \left( 2\dot{r}\dot{\theta} + r\ddot{\theta} \right) \right) \\ \ddot{y} &= \cos \phi \left( 2r\dot{\theta}\dot{\phi} \cos \theta + \left( 2\dot{r}\dot{\phi} + r\ddot{\phi} \right) \sin \theta \right) \\ &\quad + \sin \phi \left( 2\dot{r}\dot{\theta} \cos \theta + r\ddot{\theta} \cos \theta + \sin \theta \left( \ddot{r} - r\dot{\theta}^2 - r\dot{\phi}^2 \right) \right) \\ \ddot{z} &= \cos \phi \left( \ddot{r} - r\dot{\phi}^2 \right) - \sin \phi \left( 2\dot{r}\dot{\phi} + r\ddot{\phi} \right). \end{aligned} \quad (51)$$

Recall the kinetic energy form of a continuum body (§ V)

$$T = \frac{1}{2} \rho \mathbf{v}(\mathbf{r}, t) \cdot \mathbf{v}(\mathbf{r}, t) = \frac{1}{2} \rho \|\dot{\mathbf{r}}\|^2. \quad (52)$$

The constitutive equation that governs the Cauchy stress tensor,  $\boldsymbol{\sigma}$  is independent of the path of the deformation from the reference configuration and it is solely a function of the state of deformation; we therefore conclude that the IAB material is Cauchy elastic [16, §4.2]. We therefore choose  $V = 0$  following [16]'s recommendation. Since we are treating an incompressible material, the material mass density is uniform throughout the body in its configuration. Thus the rate of change of  $\rho$  vanishes. We have

$$T = \frac{1}{2} \rho \|\dot{\mathbf{r}}\|^2 = \frac{1}{2} \rho \left( \dot{r}^2 + r^2 \dot{\phi}^2 + r^2 \dot{\theta}^2 \sin^2 \phi \right), \quad V = 0. \quad (53)$$

It follows that the Lagrangian is

$$L(\mathbf{r}, \dot{\mathbf{r}}) = \frac{1}{2} \rho \left( \dot{r}^2 + r^2 \dot{\phi}^2 + r^2 \dot{\theta}^2 \sin^2 \phi \right). \quad (54)$$

and the derivatives of the canonical momenta are

$$\frac{d}{dt} \frac{\partial L}{\partial \dot{r}} = \frac{d}{dt} (\rho \dot{r}) = \rho \ddot{r} \quad (55a)$$

$$\begin{aligned} \frac{d}{dt} \frac{\partial L}{\partial \dot{\theta}} &= \frac{d}{dt} \left( r^2 \rho \dot{\theta} \sin^2 \phi \right) = 2 \rho r \dot{r} \dot{\theta} \sin^2 \phi \\ &\quad + 2 \rho r^2 \dot{\phi} \dot{\theta} \sin \phi \cos \phi + \rho r^2 \ddot{\theta} \sin^2 \phi \end{aligned} \quad (55b)$$

$$\frac{d}{dt} \frac{\partial L}{\partial \dot{\phi}} = \frac{d}{dt} \left( r^2 \rho \dot{\phi} \right) = 2 \rho \dot{r} r \dot{\phi} + \rho r^2 \ddot{\phi} \quad (55c)$$

with the following associated generalized forces

$$\begin{aligned} \frac{\partial L}{\partial r} &= \rho r \dot{\phi}^2 + \rho r \dot{\theta}^2 \sin^2 \phi, \quad \frac{\partial L}{\partial \theta} = 0, \\ \frac{\partial L}{\partial \phi} &= \rho r^2 \dot{\theta}^2 \cos \phi \sin \phi. \end{aligned} \quad (56a)$$

So that we may write the general system dynamics as

$$\begin{aligned} \boldsymbol{\tau} &= \rho \left\{ \ddot{r} + r \left[ r \ddot{\phi} + 2\dot{r} \left( \dot{\phi} + \dot{\theta} \sin^2 \phi \right) \right. \right. \\ &\quad \left. \left. + \sin \phi \left( r \ddot{\theta} \sin \phi - \dot{\theta}^2 (r \cos \phi + \sin \phi) \right) \right. \right. \\ &\quad \left. \left. + \dot{\phi} \left( -\dot{\phi} + r \dot{\theta} \sin 2\phi \right) \right] \right\} \end{aligned} \quad (57)$$

or in matrix form

$$\begin{aligned} \boldsymbol{\tau} &= \begin{bmatrix} \rho & 0 & 0 \\ 0 & \rho r^2 & 0 \\ 0 & 0 & \rho r^2 \sin^2 \phi \end{bmatrix} \begin{bmatrix} \ddot{r} \\ \ddot{\phi} \\ \ddot{\theta} \end{bmatrix} \\ &\quad + \text{diag} \begin{bmatrix} 2 \rho r \left( \dot{\theta} \sin^2 \phi + \dot{\phi} \right) \\ \rho r \left( r \dot{\theta} \sin 2\phi - \dot{\phi} \right) \\ -\rho r \dot{\theta} \sin \phi (r \cos \phi + \sin \phi) \end{bmatrix} \begin{bmatrix} \dot{r} \\ \dot{\phi} \\ \dot{\theta} \end{bmatrix}. \end{aligned} \quad (58)$$

## APPENDIX B DERIVATION OF IAB-HEAD CONTACT KINEMATICS

Here, we formulate the contact kinematics between an IAB and the head in a fashion similar to the single finger soft contact type postulated in [19]. We note that an alternative derivation that is more concise can be found in [13].

### A. Contact Coordinates and Gaussian Map

Following equations (14a), (14b), and 15, we write

$$R f_1(\alpha_1) + p = f_h(\alpha_h) \quad (59a)$$

$$R n_1(\alpha_1) = -n_h(\alpha_h) \quad (59b)$$

$$R \frac{\partial f_1}{\partial \alpha_1} M_1^{-1} R_\psi = \frac{\partial f_h}{\partial \alpha_h} M_h^{-1}. \quad (59c)$$

Differentiating (59a) and (59b), we find that

$$\dot{R} f_1(\alpha_1) + R \frac{\partial f_1}{\partial \alpha_1} \dot{\alpha}_1 + \dot{p} = \frac{\partial f_h}{\partial \alpha_h} \dot{\alpha}_h \quad (60)$$

$$\dot{R} n_1(\alpha_1) + R \frac{\partial n_1}{\partial \alpha_1} \dot{\alpha}_1 = -\frac{\partial n_h}{\partial \alpha_h} \dot{\alpha}_h. \quad (61)$$

It follows through the multiplication of (60) by  $\frac{\partial f_h}{\partial \alpha_h}^T$  and putting  $\alpha_h$  into (61), we have

$$\begin{aligned} \dot{R} n_1(\alpha_1) + R \frac{\partial n_1}{\partial \alpha_1} \dot{\alpha}_1 &= -\frac{\partial n_h}{\partial \alpha_h} M_h^{-2} \frac{\partial f_h}{\partial \alpha_h}^T \\ &\quad \left( \dot{R} f_1(\alpha_1) + R \frac{\partial f_1}{\partial \alpha_1} \dot{\alpha}_1 + \dot{p} \right). \end{aligned} \quad (62)$$

Now, putting (59c) into (62) and rearranging, we find that

$$\begin{aligned} \left[ R \frac{\partial n_1}{\partial \alpha_1} + \frac{\partial n_h}{\partial \alpha_h} M_h^{-2} \left( \frac{\partial f_h^T}{\partial \alpha_h} \frac{\partial f_h}{\partial \alpha_h} \right) M_h^{-1} R_\psi M_1 \right] \dot{\alpha}_1 \\ = -\dot{R} n_1 - \frac{\partial n_h}{\partial \alpha_h} M_h^{-2} \frac{\partial f_h}{\partial \alpha_h}^T \left( \dot{R} f_1(\alpha_1) + \dot{p} \right). \end{aligned} \quad (63)$$



Multiplying throughout by  $M_h^{-T} \frac{\partial f_h}{\partial \alpha_h}^T$ , we have on the left hand side of the above as,

$$M_h^{-T} \frac{\partial f_h}{\partial \alpha_h}^T \left( R \frac{\partial n_1}{\partial \alpha_1} + \frac{\partial n_h}{\partial \alpha_h} M_h^{-1} R_\psi M_1 \right) \dot{\alpha}_1. \quad (64)$$

Since

$$\begin{aligned} M_h^{-T} \frac{\partial f_h}{\partial \alpha_h}^T &= \frac{\partial f_h}{\partial \alpha_h} M_h^{-1} = \left( R \frac{\partial f_1}{\partial \alpha_1} M_1^{-1} R_\psi \right)^T \\ &= R_\psi M_1^{-T} \frac{\partial f_1}{\partial \alpha_1}^T R^T, \end{aligned} \quad (65)$$

equation (64) becomes

$$\begin{aligned} \dot{\alpha}_1 &\left( R_\psi M_1^{-T} \frac{\partial f_1}{\partial \alpha_1}^T \frac{\partial n_1}{\partial \alpha_1} + M_h^{-T} \frac{\partial f_h}{\partial \alpha_h}^T \frac{\partial n_h}{\partial \alpha_h} M_h^{-1} R_\psi M_1 \right) \\ &= \left( R_\psi M_1^{-T} \frac{\partial f_1}{\partial \alpha_1}^T \frac{\partial n_1}{\partial \alpha_1} M_1^{-1} R_\psi + M_h^{-T} \frac{\partial f_h}{\partial \alpha_h}^T \frac{\partial n_h}{\partial \alpha_h} M_h^{-1} \right) \times \\ &\quad R_\psi M_1 \dot{\alpha}_1. \end{aligned} \quad (66)$$

Setting

$$\tilde{\mathcal{K}}_1 = R_\psi M_1^{-T} \frac{\partial f_1}{\partial \alpha_1}^T \frac{\partial n_1}{\partial \alpha_1} M_1^{-1} R_\psi$$

and

$$\mathcal{K}_h = M_h^{-T} \frac{\partial f_h}{\partial \alpha_h}^T \frac{\partial n_h}{\partial \alpha_h} M_h^{-1},$$

it follows from (62) that

$$\begin{aligned} &(\tilde{\mathcal{K}}_1 + \mathcal{K}_h) R_\psi M_1 \dot{\alpha}_1 = \\ &M_h^{-T} \frac{\partial f_h}{\partial \alpha_h}^T \left[ -\dot{R} n_1 - \frac{\partial n_h}{\partial \alpha_h} M_h^{-2} \frac{\partial f_h}{\partial \alpha_h}^T (\dot{R} f_1 + \dot{p}) \right] \\ &= -M_h^{-T} \frac{\partial f_h}{\partial \alpha_h}^T \dot{R} n_1 - \mathcal{K}_h M_h^{-T} \frac{\partial f_h}{\partial \alpha_h}^T (\dot{R} f_1 + \dot{p}) \end{aligned} \quad (67)$$

so that

$$\begin{aligned} \dot{\alpha}_1 &= (\tilde{\mathcal{K}}_1 + \mathcal{K}_h)^{-1} R_\psi M_1^{-1} \times \\ &\quad \left[ \underbrace{-M_h^{-T} \frac{\partial f_h}{\partial \alpha_h}^T \dot{R} n_1}_{w_t} - \underbrace{\mathcal{K}_h M_h^{-T} \frac{\partial f_h}{\partial \alpha_h}^T (\dot{R} f_1 + \dot{p})}_{v_t} \right] \end{aligned} \quad (68)$$

or

$$\dot{\alpha}_1 = (\tilde{\mathcal{K}}_1 + \mathcal{K}_h)^{-1} R_\psi M_1^{-1} (w_t - \mathcal{K}_h v_t). \quad (69)$$

Finding the generalized velocity of the head with respect to a single IAB deformation is tantamount to finding  $(\dot{w}, v) = \dot{g} g^{-1}$ . Thus,

$$\omega_t = -M_h^{-T} \frac{\partial f_h}{\partial \alpha_h}^T (\omega \times (R n_1)) = -M_h^{-T} \frac{\partial f_h}{\partial \alpha_h}^T (n_h \times \omega) \quad (70)$$

$$v_t = M_h^{-T} \frac{\partial f_h}{\partial \alpha_h}^T (\omega \times (R f_1) + \omega \times p + v) \quad (71)$$

$$= M_h^{-T} \frac{\partial f_h}{\partial \alpha_h}^T (-f_h \times \omega + v), \quad (72)$$

where  $\omega_t$  is the head's rolling velocity projected onto the contact's tangent plane. The rotation normal to the surface is canceled by the cross product of  $\omega$  and  $n_h$ . In the same vein,  $v_t$  is the sliding velocity between the contacts, projected onto the tangent plane. Following the above construction, we find the kinematics of the contact point of the head in local coordinates is

$$\dot{\alpha}_h = M_h^{-1} (\tilde{\mathcal{K}}_1 + \mathcal{K}_h)^{-1} (\omega_t - \tilde{\mathcal{K}}_1 v_t), \quad (73)$$

where  $(\tilde{\mathcal{K}}_1 + \mathcal{K}_h)$  is the *relative curvature* [13]. It remains to solve for the relative orientation between the two local coordinates,  $\psi$ .

### B. Relative Contact Orientation and Torsion Metric Tensors

In matrix form, (59b) and (59c) can be written as,

$$R \begin{bmatrix} \frac{\partial f_1}{\partial \alpha_1} M_1^{-1} & n_1(\alpha_1) \end{bmatrix} \begin{bmatrix} R_\psi & 0 \\ 0 & -1 \end{bmatrix} = \begin{bmatrix} \frac{\partial f_h}{\partial \alpha_h} M_h^{-1} & n_h(\alpha_h) \end{bmatrix}. \quad (74)$$

Following the normalized Gaussian frame defined in (18), we can rewrite the above equation as

$$R[x_1 \ y_1 \ z_1] \bar{R}_\psi = [x_h \ y_h \ z_h]. \quad (75)$$

The total derivative of (75) yields

$$\begin{aligned} \dot{R} [x_1 \ y_1 \ z_1] \bar{R}_\psi + R [\dot{x}_1 \ \dot{y}_1 \ \dot{z}_1] \bar{R}_\psi + \\ R [x_1 \ y_1 \ z_1] \begin{bmatrix} \dot{R}_\psi & 0 \\ 0 & 0 \end{bmatrix} = \begin{bmatrix} \dot{x}_h \\ \dot{y}_h \\ \dot{z}_h \end{bmatrix}^T. \end{aligned} \quad (76)$$

Premultiplying by  $y_1^T R^T$  and then postmultiplying by  $\bar{R}_\psi \begin{pmatrix} 1 \\ 0 \\ 0 \end{pmatrix}$ , with the knowledge that  $\bar{R}_\psi \bar{R}_\psi = \mathbf{I}$ , and the identity  $y_1^T y_1 = 1$ , we find that

$$\begin{aligned} y_1^T R^T \dot{R} [x_1 \ y_1 \ z_1] \bar{R}_\psi + y_1^T [\dot{x}_1 \ \dot{y}_1 \ \dot{z}_1] \bar{R}_\psi \\ + (0 \ 1 \ 0) \begin{bmatrix} \dot{R}_\psi & 0 \\ 0 & 0 \end{bmatrix} = y_1^T R^T [\dot{x}_h \ \dot{y}_h \ \dot{z}_h] \end{aligned} \quad (77)$$

$$\begin{aligned} y_1^T R^T \dot{R} x_1 + y_1^T \dot{x}_1 + (0 \ 1 \ 0) \begin{bmatrix} \dot{R}_\psi R_\psi & 0 \\ 0 & 0 \end{bmatrix} \begin{pmatrix} 1 \\ 0 \\ 0 \end{pmatrix} \\ = y_1^T R^T [\dot{x}_h \ \dot{y}_h \ \dot{z}_h] \bar{R}_\psi \begin{pmatrix} 1 \\ 0 \\ 0 \end{pmatrix} \end{aligned} \quad (78)$$

$$\begin{aligned} y_1^T R^T \dot{R} x_1 + y_1^T \dot{x}_1 + (0 \ 1) \begin{bmatrix} 0 & \dot{\psi} \\ -\dot{\psi} & 0 \end{bmatrix} \begin{pmatrix} 1 \\ 0 \end{pmatrix} \\ = y_1^T R^T [\dot{x}_h \ \dot{y}_h \ \dot{z}_h] \bar{R}_\psi \begin{pmatrix} 1 \\ 0 \\ 0 \end{pmatrix} \end{aligned} \quad (79)$$

$$y_1^T R^T \dot{R} x_1 + y_1^T \dot{x}_1 - \dot{\psi} = y_1^T R^T [\dot{x}_h \ \dot{y}_h \ \dot{z}_h] \bar{R}_\psi \begin{pmatrix} 1 \\ 0 \\ 0 \end{pmatrix}. \quad (80)$$

From (75), we have that

$$\bar{R}_\psi^T [x_1^T \ y_1^T \ z_1^T] R^T = [x_h^T \ y_h^T \ z_h^T] \quad (81)$$

so that

$$[x_1^T \ y_1^T \ z_1^T] R^T = \bar{R}_\psi [x_h^T \ y_h^T \ z_h^T] \quad (82)$$

or

$$\begin{aligned} y_1^T R^T &= (0 \ 1 \ 0) \bar{R}_\psi [x_h^T \ y_h^T \ z_h^T] \\ &= (0 \ 1) R_\psi \begin{pmatrix} x_h^T \\ y_h^T \end{pmatrix}. \end{aligned} \quad (83)$$

It follows from (80) that

$$\begin{aligned} \dot{\psi} &= y_1^T R^T \dot{R} x_1 + y_1^T \frac{\partial x_1}{\partial \alpha_1} \dot{\alpha}_1 \\ &\quad - (0, 1) R_\psi \begin{bmatrix} x_h^T \dot{x}_h & x_h^T \dot{y}_h \\ y_h^T \dot{x}_h & y_h^T \dot{y}_h \end{bmatrix} R_\psi \begin{pmatrix} 1 \\ 0 \end{pmatrix}. \end{aligned} \quad (84)$$

Using the identities,

$$x_i^T y_i = 0, \implies \dot{x}_i^T y_i = -x_i^T \dot{y}_i = y_i^T \dot{x}_i \quad (85)$$

$$x_i^T x_i = 1, \implies \dot{x}_i^T x_i = 0, \quad (86)$$

we can rewrite (84) as

$$\begin{aligned} \dot{\psi} &= y_1^T R^T \dot{R} x_1 + y_h^T \frac{\partial x_h}{\partial \alpha_h} \dot{\alpha}_h + y_1^T \frac{\partial x_1}{\partial \alpha_1} \dot{\alpha}_1 \\ &= \omega_n + T_h M_h \dot{\alpha}_h + T_1 M_1 \dot{\alpha}_1 \end{aligned} \quad (87)$$

where

$$\begin{aligned} \omega_n &= y_1^T R^T \dot{R} x_1 = (R y_1)^T w \times (R x_1) \\ &= (R z_1)^T \omega = z_h^T \omega \end{aligned} \quad (88)$$

$$T_h = y_h^T \frac{\partial x_h}{\partial \alpha_h} M_h^{-T}, \quad T_1 = y_1^T \frac{\partial x_1}{\partial \alpha_1} M_1^{-T}. \quad (89)$$

It follows that the first, second and third equations of contact are given by (69), (73), and (87) respectively, *i.e.*

#### Equations of Contact

$$\dot{\alpha}_1 = \left( \tilde{\mathcal{K}}_1 + \mathcal{K}_h \right)^{-1} R_\psi M_1^{-1} (\omega_t - \mathcal{K}_h v_t) \quad (90a)$$

$$\dot{\alpha}_h = M_h^{-1} \left( \tilde{\mathcal{K}}_1 + \mathcal{K}_h \right)^{-1} (\omega_t - \tilde{\mathcal{K}}_1 v_t) \quad (90b)$$

$$\dot{\psi} = \omega_n + T_h M_h \dot{\alpha}_h + T_1 M_1 \dot{\alpha}_1. \quad (90c)$$

#### APPENDIX C

##### CONTACT-BASED BOUNDARY VALUE PROBLEM

With the spherically symmetric, and we expect that the shear stress contributions  $\sigma_{r\phi}$ ,  $\sigma_{r\theta}$ ,  $\sigma_{\phi\theta}$  vanish in (4) so that we have

$$\frac{1}{r^2} \frac{\partial}{\partial r} (r^2 \sigma_{rr}) - \frac{1}{r} (\sigma_{\theta\theta} + \sigma_{\phi\phi}) + \rho b_r = \rho \ddot{r}_x \quad (91a)$$

$$\frac{1}{r \sin \phi} \frac{\partial}{\partial \phi} (\sin \phi \sigma_{\phi\phi}) - \frac{\cot \phi}{r} (\sigma_{\theta\theta}) + \rho b_\phi = \rho \ddot{r}_y \quad (91b)$$

$$\frac{1}{r \sin \phi} \frac{\partial}{\partial \theta} (\sigma_{\theta\theta}) + \rho b_\theta = \rho \ddot{r}_z \quad (91c)$$

where the mass density  $\rho$  is uniform throughout the body and the components  $\ddot{r}_x$ ,  $\ddot{r}_y$ , and  $\ddot{r}_z$  are as given in (55). Solving the equations in (91), we have from (91a),

$$\begin{aligned} \frac{\partial \sigma_{rr}}{\partial r} &= \rho \ddot{r}_x + \frac{1}{r} (\sigma_{\theta\theta} + \sigma_{\phi\phi}) - \rho b_r \\ &= \frac{1}{r} (\sigma_{\theta\theta} + \sigma_{\phi\phi}) - \rho b_r \\ &\quad + \rho \cos \theta \left( 2\dot{r}\dot{\phi} \cos \theta + r \cos \theta \ddot{\phi} - 2r\dot{\theta}\dot{\phi} \sin \theta \right) \\ &\quad - \rho \sin \theta \left( \cos \theta (-\ddot{r} + r\dot{\theta}^2 + r\dot{\phi}^2) + \sin \theta (2\dot{r}\dot{\theta} + r\ddot{\theta}) \right) \end{aligned} \quad (92)$$

and from (91b), we have

$$\begin{aligned} \rho \ddot{r}_y &= \frac{\cot \phi}{r} (\sigma_{\phi\phi} - \sigma_{\theta\theta}) + \rho b_\phi + \frac{1}{r} \frac{\partial \sigma_{\phi\phi}}{\partial \phi} \\ \frac{\partial \sigma_{\phi\phi}}{\partial \phi} &= r \rho \ddot{r}_y - r \rho b_\phi. \end{aligned}$$

so that

$$\begin{aligned} \frac{\partial \sigma_{\phi\phi}}{\partial \phi} &= -\rho r b_\theta + r \rho \left[ \cos \phi \left( 2r\dot{\theta}\dot{\phi} \cos \theta + (2\dot{r}\dot{\phi} + r\ddot{\phi}) \sin \theta \right) + \right. \\ &\quad \left. \sin \theta \left( 2\dot{r}\dot{\phi} \cos \theta + r\ddot{\theta} \cos \theta + (\ddot{r} - r\dot{\theta}^2 - r\dot{\phi}^2) \right) \sin \phi \right] \end{aligned} \quad (93)$$

and lastly, we have from (91c)

$$\begin{aligned} \frac{\partial \sigma_{\theta\theta}}{\partial \theta} &= (\rho \ddot{r}_z - \rho b_\theta) r \sin \phi \\ &= -r \rho b_\theta \sin \phi + r \rho \sin \phi \cos \phi \left( \ddot{r} - r\dot{\phi}^2 \right) \\ &\quad - r \rho \sin^2 \phi \left( 2\dot{r}\dot{\phi} + r\ddot{\phi} \right). \end{aligned} \quad (94)$$

Collecting  $\frac{\partial \sigma_{rr}}{\partial r}$ ,  $\frac{\partial \sigma_{\theta\theta}}{\partial \theta}$ , and  $\frac{\partial \sigma_{\phi\phi}}{\partial \phi}$  above, taking  $\sigma_{rr}(r_o) = \sigma_{\theta\theta}(2\pi) = \sigma_{\phi\phi}(\pi) = 0$  and integrating from the internal to outer boundary conditions given by

$$\sigma_{rr}|_{R=R_o} = -P_{\text{atm}}, \quad \sigma_{rr}|_{R=R_i} = -P_{\text{atm}} - P \quad (95)$$

we have the full form of the normal stress components as

$$\begin{aligned} \sigma_{rr}(\delta) &= - \int_\delta^{r_o} \left[ \frac{1}{r} \left( -2p + 2C_1 \frac{r^2}{R^2} - 2C_2 \frac{R^8}{r^8} \right) - \rho b_r \right. \\ &\quad + \rho \cos \theta \left( 2\dot{r}\dot{\phi} \cos \theta + r \cos \theta \ddot{\phi} - 2r\dot{\theta}\dot{\phi} \sin \theta \right) \\ &\quad \left. - \rho \sin \phi \left( \cos \theta (-\ddot{r} + r\dot{\theta}^2 + r\dot{\phi}^2) + \sin \theta (2\dot{r}\dot{\theta} + r\ddot{\theta}) \right) \right] dr, \end{aligned} \quad (96)$$

$$\begin{aligned} \sigma_{\phi\phi}(\epsilon) &= - \int_\epsilon^\pi \left[ r \rho \left[ \cos \phi \left( 2r\dot{\theta}\dot{\phi} \cos \theta + (2\dot{r}\dot{\phi} + r\ddot{\phi}) \sin \theta \right) + \right. \right. \\ &\quad \left. \left. \sin \theta \sin \phi \left( 2\dot{r}\dot{\phi} \cos \theta + r\ddot{\theta} \cos \theta + (\ddot{r} - r\dot{\theta}^2 - r\dot{\phi}^2) \right) \right] \right. \\ &\quad \left. - \rho r b_\theta \right] d\phi \end{aligned}$$

$$\begin{aligned} \sigma_{\theta\theta}(\zeta) &= - \int_\zeta^{2\pi} \left[ -r \rho b_\theta \sin \phi + r \rho \sin \phi \cos \phi \left( \ddot{r} - r\dot{\phi}^2 \right) - \right. \\ &\quad \left. r \rho \sin^2 \phi \left( 2\dot{r}\dot{\phi} + r\ddot{\phi} \right) \right] d\theta \end{aligned} \quad (97)$$

where  $r_i \leq \delta \leq r_o$ ,  $0 \leq \epsilon \leq \pi$  and  $0 \leq \zeta \leq 2\pi$ . Now, using the boundary condition,  $P + P_{\text{atm}} = -\sigma_{rr}|_{r=r_i}$ , where  $P_{\text{atm}}$  is the atmospheric pressure, (here, taken as 0), we have the internal pressure in the IAB cavity as a function of the radius of deformation in the current configuration as

$$P = \int_{r_i}^{r_o} \left[ \frac{1}{r} \left( -2p + 2C_1 \frac{r^2}{R^2} - 2C_2 \frac{R^8}{r^8} \right) - \rho b_r + \rho \cos \theta \left( 2\dot{r}\dot{\phi} \cos \theta + r \cos \theta \ddot{\phi} - 2r\dot{\theta}\dot{\phi} \sin \theta \right) - \rho \sin \phi \left( \cos \theta (-\ddot{r} + r\dot{\theta}^2 + r\dot{\phi}^2) + \sin \theta (2\dot{r}\dot{\theta} + r\ddot{\theta}) \right) \right] dr. \quad (98)$$

## ACKNOWLEDGMENT

The authors would like to thank Erik Pearson for kindly providing the CAD models of the couch and gantry used in our SOFA model.

## REFERENCES

- [1] O. Ogunmolu, X. Liu, and R. Wiersma, "Mechanism and Constitutive Model of a Continuum Robot for Head and Neck Cancer Radiotherapy." [1](#), [2](#), [3](#), [4](#)
- [2] O. P. Ogunmolu, "A Multi-DOF Soft Robot Mechanism for Patient Motion Correction and Beam Orientation Selection in Cancer Radiation Therapy." Ph.D. dissertation, The University of Texas at Dallas; The University of Texas Southwestern Medical Center, 2019. [1](#), [3](#), [5](#)
- [3] F. M. Khan, J. P. Gibbons, and P. W. Sperduto, *Khan's Treatment Planning in Radiation Oncology*. Lippincott Williams & Wilkins, 2016. [1](#)
- [4] M. Giorrelli, F. Renda, M. Calisti, A. Arienti, G. Ferri, and C. Laschi, "Neural Network And Jacobian Method For Solving The Inverse Statics Of A Cable-driven Soft Arm With Nonconstant Curvature," *IEEE Transactions on Robotics*, vol. 31, no. 4, pp. 823–834, 2015. [1](#)
- [5] O. Ogunmolu, A. Kulkarni, Y. Tadesse, X. Gu, S. Jiang, and N. Gans, "Soft-neuroadapt: A 3-dof neuro-adaptive patient pose correction system for frameless and maskless cancer radiotherapy," in *IEEE/RSJ International Conference on Intelligent Robots and Systems (IROS)*, Vancouver, BC, CA. IEEE, 2017, pp. 3661–3668. [1](#)
- [6] H. Mochiyama, "Hyper-flexible robotic manipulators," in *IEEE International Symposium on Micro-NanoMechatronics and Human Science*, 2005. IEEE, 2005, pp. 41–46. [1](#)
- [7] G. S. Chirikjian and J. W. Burdick, "The kinematics of hyper-redundant robot locomotion," *IEEE transactions on robotics and automation*, vol. 11, no. 6, pp. 781–793, 1995. [1](#)
- [8] F. Renda and L. Seneviratne, "A Geometric and Unified Approach for Modeling Soft-Rigid Multi-body Systems with Lumped and Distributed Degrees of Freedom," *2018 IEEE International Conference on Robotics and Automation (ICRA)*, pp. 1567 – 1574, 2018. [1](#)
- [9] H. Demirkoparan and T. J. Pence, "Swelling of an Internally Pressurized Nonlinearly Elastic Tube with Fiber Reinforcing," *International journal of solids and structures*, vol. 44, no. 11-12, pp. 4009–4029, 2007. [1](#)
- [10] T. George Thuruthel, Y. Ansari, E. Falotico, and C. Laschi, "Control Strategies for Soft Robotic Manipulators: A Survey," *Soft Robotics*, vol. 5, no. 2, pp. 149–163, 2018. [1](#)
- [11] F. Faure, C. Duriez, H. Delingette, J. Allard, B. Gilles, S. Marchesseau, H. Talbot, H. Courtecuisse, G. Bousquet, I. Peterlik, and S. Cotin, "SOFA: A Multi-Model Framework for Interactive Physical Simulation," in *Soft Tissue Biomechanical Modeling for Computer Assisted Surgery*, ser. Studies in Mechanobiology, Tissue Engineering and Biomaterials, Y. Payan, Ed. Springer, June 2012, vol. 11, pp. 283–321. [Online]. Available: <https://hal.inria.fr/hal-00681539> [2](#)
- [12] V.-D. Nguyen, "Constructing force-closure grasps," *The International Journal of Robotics Research*, vol. 7, no. 3, pp. 3–16, 1988. [2](#)
- [13] D. J. Montana, "The Kinematics of Contact And Grasp," *The International Journal of Robotics Research*, vol. 7, no. 3, pp. 17–32, 1988. [2](#), [5](#), [8](#), [9](#)
- [14] M. Mooney, "A theory of large elastic deformation," *Journal of applied physics*, vol. 11, no. 9, pp. 582–592, 1940. [3](#)
- [15] A. Gent, *Engineering with Rubber. How to Design Rubber Components*. Munich: Carl Hanser Verlag Publicationbs, 2012. [3](#)
- [16] R. Ogden, *Non-linear Elastic Deformations*. Mineola, New York: Dover Publicationbs, Inc., 1997. [3](#), [4](#), [6](#), [7](#), [8](#)
- [17] O. Ogunmolu, E. Pearson, X. Liu, and R. Wiersma, "Kinematics and Dynamics of a Continuum Robot Immobilization Mechanism for Cancer Radiotherapy," *Submitted to IEEE Transactions on Robotics*, 2019., 2019. [Online]. Available: [scriptedonachip.com/downloads/Papers/ContinuumII.pdf](https://scriptedonachip.com/downloads/Papers/ContinuumII.pdf)
- [18] M. Spivak, "A Comprehensive Introduction to Differential Geometry. Vol. V. Berkeley: Publish or Perish," *Inc. XI*, 1979. [5](#)
- [19] R. M. Murray and S. Sastry, "Grasping and Manipulation using Multifingered Robot Hands." in *Proceedings of Symposia in Applied Mathematics*, vol. 41, 1990, pp. 329–335. [5](#), [6](#), [8](#)
- [20] J. R. Kerr, "An Analysis of Multi-Fingered Hands," *International Journal of Robotics Research*, no. Dept. of Mechanical Engineering, pp. 3–17, 1984. [Online]. Available: <http://journals.sagepub.com/doi/pdf/10.1177/027836498600400401> [6](#)
- [21] C. Truesdell and W. Noll, *The Non-Linear Field Theories of Mechanics*. Springer, 1965. [6](#)